Available online at www.sciencedirect.com
SCIENCE DIRECT®
Optical Materials 21 (2003) 705–712
OPTICAL Materials
www.elsevier.com/locate/optmat

Absorption and emission spectroscopy in Er^{3+}–Yb^{3+} doped aluminum oxide waveguides

Christof Strohhöfer *, Albert Polman

FOM Institute for Atomic and Molecular Physics, Kruislaan 407, 1098 SJ Amsterdam, The Netherlands

Received 15 March 2001; accepted 2 May 2002

Abstract

The spectroscopic properties of Al_2O_3 waveguides ion implanted with Er^{3+} and Yb^{3+} are investigated in view of their application in optical amplifiers operating at 1530 nm. Absorption cross-sections are obtained by means of waveguide transmission experiments, taking into account the overlap between optical mode and doped region of the waveguide. Emission cross-sections for the Er^{3+}:$^4I_{13/2}$ and Yb^{3+}:$^2F_{5/2}$ levels are calculated from the absorption cross-sections. The rate coefficient for energy transfer between Yb^{3+} and Er^{3+} under excitation around 980 nm is estimated by emission intensity and decay rate measurements. It amounts to approximately 3.6×10^{-17} cm^3/s for concentrations of 0.29 at.% erbium and 0.28 at.% ytterbium.

PACS: 42.70.Hj; 42.82.Gw
Keywords: Erbium; Ytterbium; Codoping; Al_2O_3; Waveguide; Energy transfer

1. Introduction

Erbium-doped amplifiers are by now an indispensable element in optical fibre telecommunications systems. They are able to provide high gain in the spectral region around 1530 nm, where silica fibres have their transmission maximum. In the field of miniature integrated optics, erbium-doped waveguide amplifiers [1–5] have proven their ability to provide optical gain over short distances. The first generation of integrated amplifiers used mainly laser diodes emitting at 1480 nm for optical pumping. Under this excitation scheme, the metastable $^4I_{13/2}$ level of the erbium ions is excited directly via its high-lying Stark states. The ions act as a quasi-three-level laser system, which limits the population inversion with respect to the ground state to roughly 40% (corresponding to a population in the first excited state of 70%) because of stimulated emission by pump radiation. On the other hand, when pumping into the second excited state $^4I_{11/2}$ using 980 nm radiation, a population inversion between metastable level and ground state of close to 100% can be obtained.

This second excitation scheme of Er^{3+} in waveguide amplifiers requires considerably higher intensities, since the absorption cross-section of the

* Corresponding author. Tel.: +31-20-6081234; fax: +31-20-6684106.
E-mail address: c.strohhofer@amolf.nl (C. Strohhöfer).

0925-3467/03/$ - see front matter
PII: S0925-3467(02)00056-3

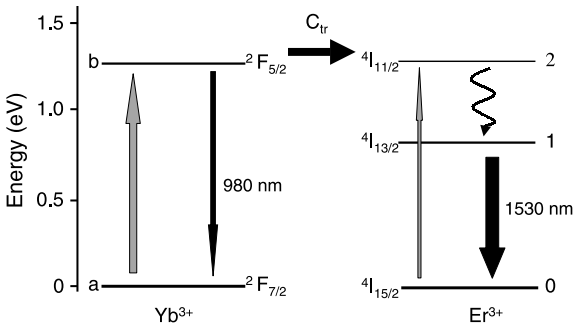

Fig. 1. Schematic of the energy transfer process between Yb^{3+} and Er^{3+}. Excitation takes place around 980 nm and can excite both erbium and ytterbium. Yb^{3+} can either decay to its ground state or transfer its energy to the Er^{3+} $^4I_{11/2}$ level. Within the erbium, decay of the $^4I_{11/2}$ state to the $^4I_{13/2}$ state leads to a build-up of population in the metastable $^4I_{13/2}$ level.

$^4I_{11/2}$ state is small. The excitation cross-section of Er^{3+} around 980 nm can however be increased by codoping with ytterbium (cf. Fig. 1 for a schematic of the process). The absorption cross-section of Yb^{3+} at 980 nm is about an order of magnitude larger than that of Er^{3+}, and its absorption band extends over a wider wavelength region, between 850 and 1000 nm. From Yb^{3+} the energy is then transferred resonantly to the $^4I_{11/2}$ state of Er^{3+}. This energy transfer has been investigated in a wide range of materials, both glassy and crystalline (see e.g. Refs. [6–10]). Based on this excitation scheme, an integrated amplifier in phosphate glass has been reported [11].

Important characteristics of amplifier materials are their optical absorption and emission cross-sections. They determine, in conjunction with the efficiency of the energy transfer between Yb^{3+} and Er^{3+}, the maximum gain and pumping efficiency of an amplifier. The cross-sections of rare earth ions are too small to be easily obtained by standard normal-incidence spectroscopy in thin film structures. Transmission experiments through waveguides increase the interaction length of the light with the dopant ions, and therefore the total absorbance. For samples where only the guiding region is doped, several research groups have shown that absorbance spectra of the dopants can be obtained in this way [12,13], yet the results are all of a qualitative nature.

In this article, we will investigate the absorption and emission properties of Er^{3+} and Yb^{3+} in Al_2O_3. Aluminum oxide has already been reported as a suitable host medium for Er^{3+}-doped optical waveguide amplifiers [3]. It has also been shown that in this material energy transfer between Yb^{3+} and Er^{3+} [14] takes place. We need to obtain, however, quantitative data that will allow us to estimate whether ytterbium codoping will lead to an improvement in amplifier performance. To this end we will address two types of questions associated with a waveguide amplifier codoped with Er^{3+} and Yb^{3+}: in the first part we will obtain absolute values for the absorption cross-sections from waveguide transmission measurements and calculate the relevant emission cross-sections. In the second part we will determine the efficiency of the energy transfer between Yb^{3+} and Er^{3+} from measurements of emitted intensities from the Er^{3+} $^4I_{13/2}$ state, and independently from measurements of Yb^{3+} decay rates.

2. Experimental

Aluminum oxide films were deposited on thermally oxidized silicon wafers by RF-sputtering [15,16]. The thickness of the Al_2O_3 and SiO_2 layers was 500 nm and 5 μm respectively. Erbium and ytterbium were introduced into the Al_2O_3 film by ion implantation at energies ranging from 1800 to 200 keV, creating a flat dopant profile throughout most of the film. The dopant concentrations were determined by Rutherford backscattering spectrometry (RBS) and amount to 3.35×10^{20} Er/cm^3 (0.29 at.%) and 3.28×10^{20} Yb/cm^3 (0.28 at.%). Besides the sample doped with erbium and ytterbium, samples containing only erbium or ytterbium were prepared. For reference purposes, a piece was kept unimplanted.

Straight waveguides of widths ranging from 1 to 3.5 μm were defined by standard photolithographic techniques. Ridges were etched to a depth of approximately 200 nm with an argon atom beam. Subsequently a cover layer of 1.35 μm SiO_2 was sputtered onto the waveguides. The samples were cut to a length of 8 mm and the cleaved edges

were mechanically polished. Finally they were annealed in vacuum for an hour at 775 °C.

The exact shape of the waveguides was determined using scanning electron microscopy on typical waveguide samples before the deposition of the cover layer. The acceleration voltage for these measurements was 15 kV.

Waveguide transmission measurements were performed by coupling white light from a halogen lamp into one facet of a waveguide with the help of a lensed fibre. The transmitted signal was collected at the output facet with a 40× microscope objective and focussed onto the tip of a fibre with a core diameter of 800 μm. The collected light was dispersed in a 96 cm monochromator and detected with a thermoelectrically cooled AgOCs photomultiplier tube in the spectral region between 400 and 1100 nm, and with a liquid nitrogen cooled germanium detector in the region from 1100 to 1700 nm. Standard lock-in techniques were used to decrease the noise level. The wavelength resolution of these measurements is approximately 3 nm.

To obtain photoluminescence spectra and decay curves of Er^{3+} and Yb^{3+}, the ions were excited with a continuous wave titanium sapphire laser, tunable in the range from 890 to 1030 nm. The pump radiation was mechanically chopped and coupled into the waveguide from an optical fibre. The photoluminescence signal was detected perpendicular to the waveguide through the top cladding using a fibre with an 800 μm core. The detection system was the same as described above. The AgOCs photomultiplier tube was used to measure the Yb^{3+} emission at wavelengths around 1000 nm, and the germanium detector to measure the photoluminescence of Er^{3+} around 1530 nm. Decay curves for the Er^{3+} emission were recorded using a digital oscilloscope, for the Yb^{3+} emission using a photon counting system. The time response of the detection set-up was 40 μs. Special care has been taken to ensure that all measurements were performed at excitation densities where both the Yb^{3+} and Er^{3+} emission intensities are in the regime linear with pump power.

To obtain a calibration of the photoluminescence intensity at 1530 nm of erbium-only and erbium–ytterbium doped Al_2O_3 relative to each other under 980 nm excitation, spectra of the $^4I_{13/2}$ emission were taken in standard photoluminescence geometry: the excitation beam was incident onto the sample surface under an angle of 30°, and the emitted light was focussed onto the entrance slit of the monochromator.

3. Waveguide absorption measurements

The transmission of a 3.5 μm wide waveguide doped with Er^{3+} and a 2.5 μm wide waveguide doped with Yb^{3+} was measured as a function of wavelength. As reference served the spectrum of transmitted intensity through an undoped waveguide. In this way the effects of absorption by the rare earths can be extracted from a signal which also contains the effects of the waveguiding properties of the structure itself. Since scattering effects can be excluded in this way, the transmission data is converted to absorbance assuming a Lambert–Beer dependency. The absorption cross-section is related to the absorbance through

$$\sigma_{\mathrm{abs}}(\lambda) = \frac{A(\lambda)}{\eta_{\mathrm{overlap}}(\lambda) N_{\mathrm{abs}} l} \tag{1}$$

where σ_{abs} is the absorption cross-section; A, the absorbance; η_{overlap}, the overlap between waveguide mode and doped region; and N_{abs} and l, the concentration of the dopant and the length of the waveguide respectively.

To obtain absolute values for the absorption cross-section in waveguide transmission measurements, it is important to know the exact cross-section of the waveguide and the development of the mode shape with wavelength over the range investigated.

Fig. 2 shows a scanning electron microscopy image of the cross-section of a nominally 2 μm wide waveguide. Included is a contour profile of the fundamental mode for 980 nm radiation calculated numerically using a finite difference algorithm. Although the image shows a waveguide without the SiO_2 cover layer for better contrast, the calculation has been performed taking account of the final geometry including the cover layer. For all waveguide widths used in the transmission measurements, mode profiles were calculated for several wavelengths, taking into consideration the

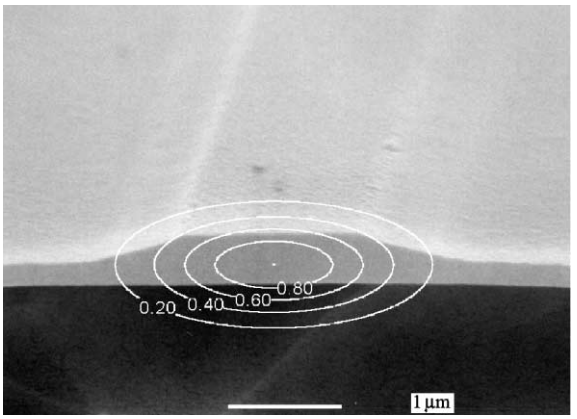

Fig. 2. Scanning electron microscopy image of the cross-section of an Al_2O_3 ridge waveguide with nominal width 2 μm. The image was taken before the deposition of the SiO_2 cover layer. The SiO_2 buffer layer underneath the Al_2O_3 waveguide appears black. Included is the intensity contour plot of the fundamental mode at 980 nm for the complete waveguide structure, calculated by a finite difference method. The overlap between mode and doped region of the waveguide has to be taken into account to obtain absolute cross-section values from waveguide transmission measurements.

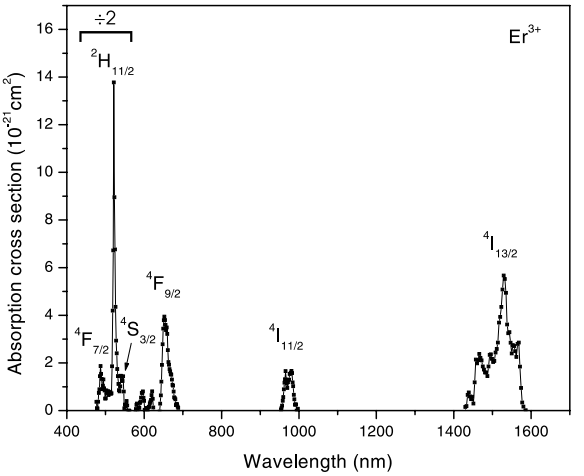

Fig. 3. Absorption cross-sections of Er^{3+} obtained from waveguide transmission experiments. Transitions are from the ground state to the indicated excited states. The absorption of the $^4I_{9/2}$ level was below the sensitivity of our measurement. Note that the absorption cross-section in the wavelength range 475–560 nm has been reduced by a factor of two.

dispersion of SiO_2 and Al_2O_3. The calculated profiles were approximated by two-dimensional Gaussian functions, and integrated over the dopant profile, measured by RBS, and the waveguide profile to obtain the overlap η_{overlap}. A second order polynomial was used to describe phenomenologically the functional dependence of η_{overlap} with wavelength.

Although great care was taken to ensure that only the fundamental mode was present, it is possible that higher order modes propagate in the waveguide during measurement. These higher order modes have a smaller overlap with the doped core of the waveguide than the fundamental mode, reducing their modal absorption. Therefore, for accuracy, the values we calculate from the transmission data have to be seen as lower limits to the real absorption cross-sections.

Fig. 3 shows the absorption cross-section of Er^{3+} in the Al_2O_3 waveguides determined as described above. All energy levels up to $^4F_{7/2}$ are given, and marked in the figure, except the $^4I_{9/2}$ level, expected around 800 nm, whose absorbance was below the accuracy of our measurement. The highest absorption cross-section occurs at 521 nm, belonging to the $^2H_{11/2}$ level. The error on the peak cross-section in this case amounts to 1×10^{-20} cm^2, considerably larger than the error on the other absorption cross-sections, since the intensity of the transmitted light is close to zero at that wavelength. The peaks around 600 nm are caused by noise in the measurement and can serve as an indication for the accuracy of the cross-section values. Note that in Fig. 3 the absorption cross-sections in the wavelength range 475–560 nm have been reduced by a factor of two. The peak cross-sections for the individual energy levels are listed in Table 1.

The measured absorption cross-section of the Yb^{3+} $^2F_{5/2}$ level is depicted in Fig. 4. At its peak, the ytterbium absorption cross-section is seven times larger than the absorption cross-section of the Er^{3+} $^4I_{11/2}$ level. In the following section we will show that this high cross-section can be used to advantage to increase the excitation rate of Er^{3+} by energy transfer from Yb^{3+}. The determination of the cross-sections from these waveguide transmission measurements is validated by the close correspondence between the absorption

Table 1
Peak absorption and emission cross-sections for Er^{3+} and Yb^{3+} energy levels

Ion	Energy level	λ_{peak} (nm)	σ_{abs} (10^{-21} cm^2)	σ_{em} (10^{-21} cm^2)
Er^{3+}	$^4I_{13/2}$	1529.0	5.7 ± 0.7	
		1532.0		5.7
	$^4I_{11/2}$	980.5	1.7 ± 0.7	
	$^4I_{9/2}$		<0.7	
	$^4F_{9/2}$	652.0	4.0 ± 0.7	
	$^4S_{3/2}$	545.5	2.9 ± 0.7	
	$^2H_{11/2}$	521.5	27.6 ± 10	
	$^4F_{7/2}$	487.0	3.7 ± 0.7	
Yb^{3+}	$^2F_{5/2}$	974.5	11.7 ± 1.0	11.6

Absorption of the given levels originates from the ground state of the ion, emission involves a transition to the ground state.

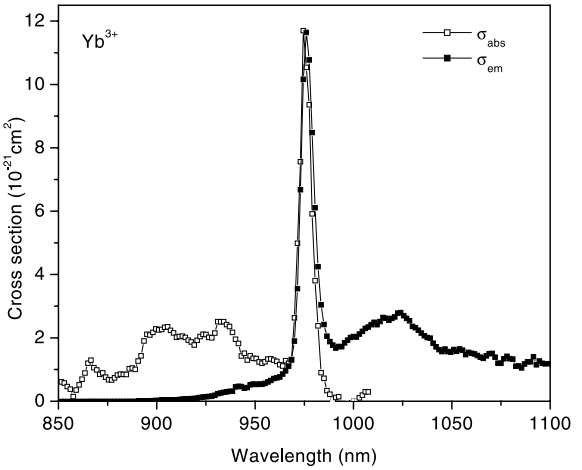

Fig. 4. Absorption and emission cross-section of the $^2F_{5/2}$ level of Yb^{3+}. The absorption cross-section was obtained from waveguide transmission measurements, the emission cross-section calculated using absorption and photoluminescence data.

cross-section values of the Er^{3+} $^4I_{13/2}$ level obtained here and by prism coupling in Ref. [17].

Using the measured absorption cross-sections, emission cross-sections from the Er^{3+} $^4I_{13/2}$ and Yb^{3+} $^2F_{5/2}$ levels to the corresponding ground states were calculated using the theory developped by McCumber [18] as applied to rare earth ions by Miniscalco and Quimby [19]. Since in both cases the measured cross-sections in the wings of the absorption lines are not sufficiently accurate to calculate the emission cross-sections, we scaled the photoluminescence emission spectra of the relevant transitions to the value of the cross-section calculated at their peak. As an example the emission cross-section of Yb^{3+} is included in Fig. 4. Numerical values of the cross-section maxima are given in Table 1.

4. Energy transfer

The effect of ytterbium codoping on the photoluminescence of Er^{3+} is depicted in Fig. 5. Two spectra of the emission from the $^4I_{13/2}$ level of Er^{3+} are shown. The more intense one originates from the sample doped with erbium and ytterbium, the weaker one from the sample doped only with erbium. The photoluminescence was excited under identical conditions using radiation at 975 nm. On ytterbium codoping, the photoluminescence is increased sixfold. The line shape of the emission remains unchanged by the introduction of ytterbium into the sample, as does the decay rate of the $^4I_{13/2}$ level, measured at 1533 nm to be 625 s^{-1}.

To obtain a qualitative impression of the excitation mechanism, we have monitored the photoluminescence from the Er^{3+} $^4I_{13/2}$ line as a function of excitation wavelength between 890 and

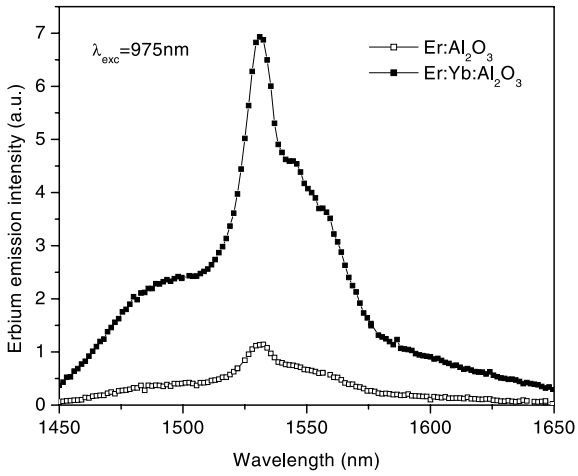

Fig. 5. Comparison of photoluminescence emission spectra of the Er^{3+} $^4I_{13/2}$ level in samples doped with erbium and with ytterbium and erbium. The emission is enhanced by a factor of six on ytterbium codoping under identical excitation conditions ($\lambda_{excitation} = 975$, $I_{excitation} = 0.5$ W/cm^2).

1030 nm. Care was taken to optimize the coupling of the excitation light into the waveguide for all wavelengths used. The excitation spectra of samples doped with erbium and erbium–ytterbium are shown in Fig. 6. In the sample without ytterbium, erbium can only be excited in a narrow band centred at 975 nm and extending from 955 to 1000 nm. This band resembles the erbium absorption cross-section shown in Fig. 3. In contrast, when the sample is codoped with ytterbium, the same emission can be excited over a much wider wavelength range, with a sharp peak at 975 nm. This peak is a characteristic of the Yb^{3+} $^2F_{5/2}$ absorption. The excitation spectrum of the erbium emission from the ytterbium codoped sample is replotted in Fig. 7, to compare it with the absorption cross-section from Fig. 4. From the fact that both spectra show the same features, we can conclude that the pump radiation is mainly absorbed by Yb^{3+}. Energy transfer from Yb^{3+} to Er^{3+} then takes place as depicted in Fig. 1. Since the absorption line of Yb^{3+} extends even to shorter wavelengths than were accessible in our excitation experiment, excitation of Er^{3+} emission is not limited to the wavelengths shown in the plot. Ref. [14] gives an excitation spectrum of Er^{3+} in erbium–ytterbium codoped Al_2O_3 between 760 and 850 nm, which we extend here to longer wavelengths. The fact that excitation of the Er^{3+} is possible even when exciting outside the Er^{3+} $^4I_{11/2}$ absorption band is evidence for a thermalisation process within the ytterbium system, possibly involving migration of excitation.

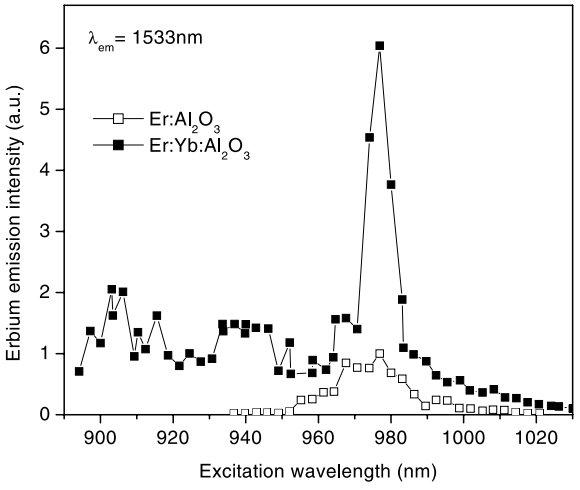

Fig. 6. Excitation spectra of the Er^{3+} $^4I_{13/2}$ emission from erbium doped Al_2O_3 and erbium–ytterbium codoped Al_2O_3.

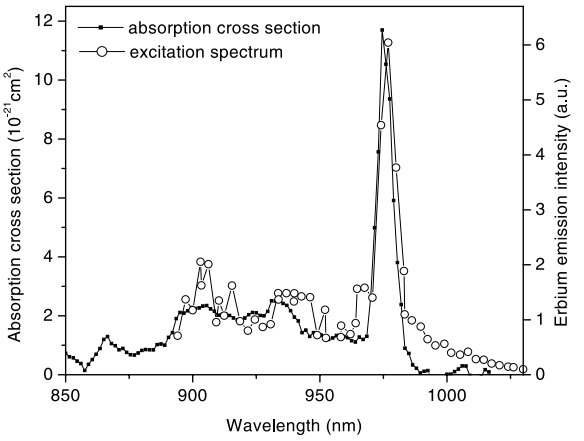

Fig. 7. Comparison of the excitation spectrum of the erbium emission at 1530 nm and the absorption cross-section of Yb^{3+} obtained by waveguide transmission experiments.

The ratio of the Er^{3+} emission intensity in the Er-doped and Er/Yb-codoped samples (compare Fig. 6) contains information about the efficiency of the energy transfer process. The rate equations in the limit of low excitation density according to the schematic Fig. 1 are:

$$\begin{aligned}\frac{dN_b}{dt} &= \sigma_{ab}\Phi_p N_{Yb} - W_b N_b - C_{tr} N_b N_{Er},\\ \frac{dN_2}{dt} &= \sigma_{02}\Phi_p N_{Er} + C_{tr} N_b N_{Er} - W_2 N_2,\\ \frac{dN_1}{dt} &= W_{21} N_2 - W_1 N_1.\end{aligned} \tag{2}$$

In these equations N_1 and N_2 represent the populations of the first and second excited state of Er^{3+}; and N_b, the population in the excited state of Yb^{3+} (cf. the labels in Fig. 1), while N_{Er} and N_{Yb} are the total erbium and ytterbium concentrations. σ_{ab} and σ_{02} signify the absorption cross-sections of Yb^{3+} and Er^{3+} at the excitation wavelength, respectively. W_1, W_2, and W_b represent the total decay rates of the corresponding levels in the absence of energy transfer, W_{21} is the transition rate from the $^4I_{11/2}$ to $^4I_{13/2}$ level in Er^{3+}; and C_{tr}, the energy

transfer coefficient. Φ_p is the photon flux density of the exciting radiation. The rate equations in absence of ytterbium are easily obtained by setting N_{Yb} and N_b zero.

C_{tr} is an effective energy transfer coefficient including forward and back energy transfer. As long as the populations of the Yb^{3+} $^2F_{5/2}$ and Er^{3+} $^4I_{11/2}$ levels are linear functions of excitation power, C_{tr} is independent of pump photon flux.

In steady state, the populations of the Er^{3+} $^4I_{13/2}$ level are given by

$$N_1^{ErYb} = \frac{W_{21}}{W_2}\frac{1}{W_1}\left(\sigma_{02}N_{Er} + \frac{C_{tr}N_{Er}}{W_b + C_{tr}N_{Er}}\sigma_{ab}N_{Yb}\right)\Phi_p,$$

$$N_1^{Er} = \frac{W_{21}}{W_2}\frac{1}{W_1}\sigma_{02}N_{Er}\Phi_p, \quad (3)$$

according to rate equations (2). Here the superscripts ErYb and Er denote the cases with ytterbium codoping and without, respectively. Assuming the radiative decay rate of the Er^{3+} $^4I_{13/2}$ level is not changed on codoping with Yb^{3+}, which is reasonable considering that the decay rate of the erbium emission does not change, the ratio R of the erbium emission intensity is given by the ratio of populations in the first excited state.

$$R = \frac{N_1^{ErYb}}{N_1^{Er}} = 1 + \frac{C_{tr}N_{Er}}{W_b + C_{tr}N_{Er}}\frac{\sigma_{ab}}{\sigma_{02}}\frac{N_{Yb}}{N_{Er}}. \quad (4)$$

The term $(C_{tr}N_{Er})/(W_b + C_{tr}N_{Er})$ is the transfer efficiency, which can be obtained from Eq. (4) since all other parameters are known (R from Fig. 6, σ_{ab} and σ_{02} from Figs. 3 and 4, N_{Yb} and N_{Er} from RBS measurements). At an excitation wavelength of 975 nm the energy transfer efficiency amounts to 0.62. This also means that 38% of the power absorbed by Yb^{3+} is lost via radiative or nonradiative processes, and not via an energy transfer to Er^{3+}. The corresponding energy transfer coefficient C_{tr} is 3.3×10^{-17} cm^3/s.

The energy transfer efficiency can independently be estimated from the Yb^{3+} $^4F_{5/2}$ decay rate. Fig. 8 shows the Yb^{3+} decay traces of a reference sample doped only with ytterbium and of the codoped sample. For these measurements, the photoluminescence was excited at 921 nm and monitored at 976 nm. The faster decay of the codoped sample is

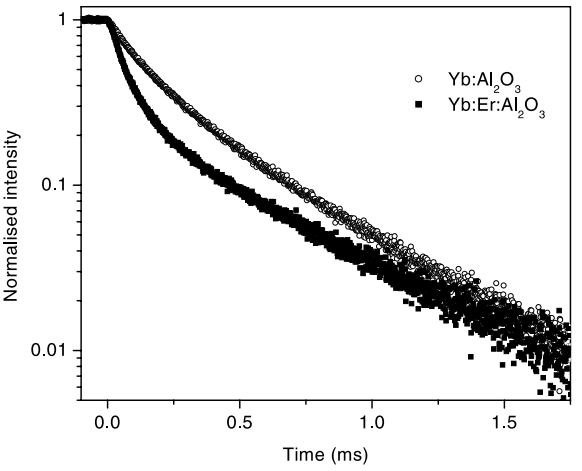

Fig. 8. Decay traces of the Yb^{3+} emission at 976 nm in ytterbium-doped and erbium/ytterbium-codoped Al_2O_3, excited with 921 nm radiation. The increase in decay rate on codoping with erbium reflects the energy transfer from Yb^{3+} to Er^{3+}.

caused by the fact that the energy transfer towards Er^{3+} constitutes an additional decay channel for Yb^{3+} in its excited state. The absence of a detector response time-limited step in the decay traces at $t = 0$ shows that decay components faster than the detector response are negligible. For single-exponential decays, the energy transfer rate is simply given by

$$W_{tr} = C_{tr}N_{Er} = W^{YbEr} - W^{Yb}. \quad (5)$$

Here W_{tr} represents the transfer rate from Yb^{3+} to Er^{3+}, and W^{YbEr} and W^{Yb} the measured Yb^{3+} $^2F_{5/2}$ decay rates in the codoped and Yb-doped samples, respectively. Both decay traces in Fig. 8, however, are multi-exponential, which has to be taken into account when calculating the transfer rates by using correct weights for the contributions to intensity of ions with different photoluminescence properties. A transfer efficiency of 0.68 ($C_{tr} = 4 \times 10^{-17}$ cm^3/s) is obtained, in close correspondence to the value calculated from Eq. (4).

5. Conclusion

In this article we have studied the spectroscopic properties of Al_2O_3 waveguides doped with Er^{3+}

and Yb^{3+}. The important parameters for application of these waveguides as optical amplifiers in the spectral region around 1530 nm are the absorption and emission cross-sections of Er^{3+} and Yb^{3+}, and the rate of the energy transfer between Yb^{3+} and Er^{3+}.

By measuring the transmission through waveguides doped with Er^{3+} and Yb^{3+} we have been able to obtain absorption cross-section data for most of the absorption lines of the two dopant ions in the spectral region between 400 and 1700 nm. Important for our procedure are an exact knowledge of the waveguiding structure and the development of the optical mode size with wavelength. From the absorption cross-section of the Er^{3+} $^4I_{13/2}$ and Yb^{3+} $^2F_{5/2}$ states, the emission cross-section of these energy levels were obtained by application of McCumber theory.

The energy transfer was investigated by both photoluminescence intensity measurements of the $^4I_{13/2}$ level of Er^{3+} and by decay rate measurements of the $^2F_{5/2}$ level of Yb^{3+}. The photoluminescence excitation spectrum of the Er^{3+} $^4I_{13/2}$ emission around 1530 nm of erbium–ytterbium codoped Al_2O_3 resembles the Yb^{3+} $^2F_{5/2}$ absorption line under excitation in the wavelength range between 890 and 1030 nm. This is clear evidence of energy transfer from Yb^{3+} to Er^{3+}. By ytterbium codoping, the Er^{3+} $^4I_{13/2}$ emission intensity is enhanced by a factor of six when excited at 975 nm. The rate coefficient for energy transfer between the Yb^{3+} $^2F_{5/2}$ and the Er^{3+} $^4I_{11/2}$ states amounts to approximately 3.6×10^{-17} cm^3/s.

Acknowledgements

We would like to acknowledge J.W.M. van Uffelen from Delft University of Technology for depositing the Al_2O_3 films, fabricating the waveguides, and Scanning Electron Microscope measurements. This work is part of the research programme of FOM, and was financially supported by NWO and IOP Electro-Optics.

References

[1] T. Kitagawa, K. Hattori, K. Shuto, M. Yasu, M. Kobayashi, M. Horiguchi, Electronics Letters 28 (1992) 1818.
[2] R.N. Ghosh, J. Shmulovich, C.F. Kane, M.R.X. de Barros, G. Nykolak, A.J. Bruce, P.C. Becker, IEEE Photonics Technology Letters 8 (1996) 518.
[3] G.N. van den Hoven, R.J.I.M. Koper, A. Polman, C. van Dam, J.W.M. van Uffelen, M.K. Smit, Applied Physics Letters 68 (1996) 1886.
[4] H.J. van Weerden, T.H. Hoekstra, P.V. Lambeck, T.J.A. Popma, in: Proceedings of the 8th European Conference on Integrated Optics, Royal Institute of Technology, Stockholm, Sweden, 1997, p. 169.
[5] Y.C. Yan, A.J. Faber, H. de Waal, P.G. Kik, A. Polman, Applied Physics Letters 71 (1997) 2922.
[6] E.F. Artem'ev, A.G. Murzin, Y.K. Fedorov, V.A. Fromzel, Soviet Journal of Quantum Electronics 11 (1981) 1266.
[7] B. Zandi, L.D. Merkle, J.A. Hutchinson, H.R. Verdun, B.H.T. Chai, Journal de Physique IV 4 (1994) C4-587.
[8] B. Simondi-Teisseire, B. Viana, D. Vivien, A.M. Lejus, Optical Materials 6 (1996) 267.
[9] M.P. Hehlen, N.J. Cockroft, T.R. Gosnell, A.J. Bruce, Physical Review B 56 (1997) 9302.
[10] E. Cantelar, J.A. Muñoz, J.A. Sanz-García, F. Cusso, Journal of Physics: Condensed Matter 10 (1998) 8893.
[11] J.-M.P. Delavaux, S. Granlund, O. Mizuhara, L.D. Tzeng, D. Barbier, M. Rattay, F. Saint André, A. Kevorkian, IEEE Photonics Technology Letters 9 (1997) 247.
[12] J.A. Lazáro, J.A. Vallés, M.A. Rebolledo, Pure and Applied Optics 7 (1998) 1363.
[13] X. Orignac, D. Barbier, X.M. Du, R.M. Almeida, O. McCarthy, E. Yeatman, Optical Materials 12 (1999) 1.
[14] C.E. Chryssou, C.W. Pitt, P.J. Chandler, D.E. Hole, IEE Proceeding, Optoelectronics 145 (1998) 325.
[15] M.K. Smit, Integrated optics in silicon-based aluminium oxide, Ph.D. Thesis, Optics Laboratory, Department of Applied Physics, Delft University of Technology, The Netherlands, 1991.
[16] M.K. Smit, C.J. van der Laan, G.A. Acket, Thin Solid Films 138 (1986) 171.
[17] G.N. van den Hoven, J.A. van der Elsken, A. Polmari, C. van Dam, J.W.M. van Uffelen, M. Srnit, Applied Optics 36 (1997) 3338.
[18] D.E. McCumber, Physical Review 136 (1964) A954.
[19] W.J. Miniscalco, R.S. Quimby, Optics Letters 16 (1991) 258.